

pubs.acs.org/crystal Article

# Understanding the Nucleation and Growth of ZIF-8 Polymorphs

A. Rain Talosig, Fangni Wang, Justin T. Mulvey, Brooke P. Carpenter, Elisa M. Olivas, Benjamin B. Katz, Chenhui Zhu, and Joseph P. Patterson\*



Cite This: Cryst. Growth Des. 2024, 24, 4136-4142



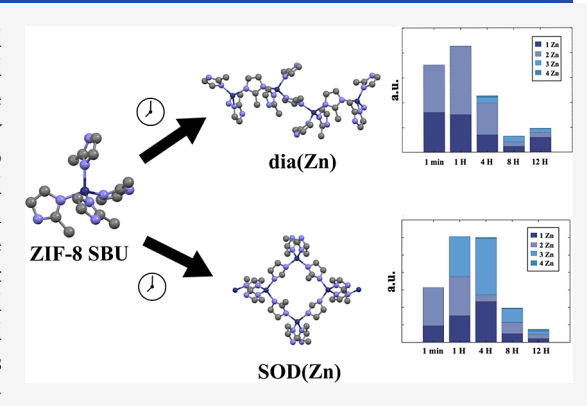
**ACCESS** I

III Metrics & More

Article Recommendations

Supporting Information

ABSTRACT: Polymorphism is an important concept in crystallization and has been widely studied for many systems, including calcium carbonate and zeolite materials. Metal-organic frameworks (MOFs) are crystalline materials that exhibit polymorphism. MOF polymorphism has been widely studied from the perspective of which synthetic factors, such as the ligand to metal ratio, can be used to control the final polymorph. However, limited studies on the nucleation mechanism of multipolymorph MOFs have been performed. Here we study the formation of a model zeolitic imidazole framework-8 and the mechanism that drives the formation of the two most commonly observed polymorphs, sodalite and diamondoid. To understand the mechanism and factors that affect polymorph formation, we performed time-resolved in situ wide-field X-ray scattering, electrospray ionization mass spectrometry, and time-resolved cryogenic transmission electron micros-



copy. The collective data reveal a clear correlation between the size of the prenucleation clusters and the final polymorph. By gaining a deeper understanding of the mechanisms governing polymorph control in MOF systems, we can improve the design of synthetic conditions, allowing the tailoring of crystal properties.

## INTRODUCTION

Metal-organic frameworks (MOFs) are a class of nanoporous materials consisting of inorganic metal nodes that are bridged by organic linkers. The MOFs have a wide range of applications due to their ultrahigh surface area, fixed porosity, and high thermal stability. MOFs can exhibit polymorphism, where the MOF structure contains identical chemical composition, but varies in network topology. 4-6 Polymorphism in MOFs can be a determining factor in function, as demonstrated by the ZIF-8 system where enhanced separation of ethane and ethene is observed for more dense ZIF-8 structures such as ZIF-8 I43m, ZIF-8 R3m, and ZIF-8 Cm.

While much work has focused on the characterization of MOF polymorphs<sup>8</sup> and the synthetic factors affecting polymorph selection, the mechanisms by which different polymorphs form have largely been unexplored. This leaves a substantial knowledge gap in our understanding of MOF nucleation and growth. 9,10 Characterizing MOF nucleation and growth is challenging due to the transient nature of the prenucleation clusters (PNCs) and amorphous phases which are commonly found in the nonclassical nucleation and growth mechanisms. 11 Currently nucleation and growth are studied through complementary methods to understand each phase and phase transition. 9,12-14 Microscopy allows for insight into final crystal morphology and size, while spectroscopy and diffraction allow for an understanding of ensemble information and crystallization kinetics. In a study by Filez et al., a molecular understanding of PNCs and crystal formation in

Zeolitic imidazolate framework -67 (ZIF-67) was unveiled using mass spectrometry, which, due to the soft analysis techniques would not deteriorate the fragile bonds in the PNCs. Furthermore, a comprehensive understanding of the nucleation and growth mechanisms attributed to the final morphology will aid in elucidating the classical and nonclassical routes of crystal growth in the MOFs. This work aims to gain an understanding of nucleation and growth of MOFs through analysis of prenucleation phases with the goal of uncovering a connection between the prenucleation stages and the final polymorph selection. Understanding this will facilitate and streamline the development of high performance MOFs without the need for high throughput synthesis and instead utilize a thorough understanding of their structure-function relationship. 15

ZIFs are a subclass of MOFs that are topologically similar to zeolites, sharing similar structures to those seen in aluminosilicate zeolite minerals. 16,17 ZIFs are composed of tetrahedrally coordinated transition metal ions that are connected by molecular imidazolate linkers. In the case of ZIF-8, the structure is formed by coordination of Zn<sup>2+</sup> ions and

Received: February 8, 2024 Revised: April 16, 2024 Accepted: April 18, 2024 Published: April 26, 2024





2-methylimidazole (HmIm). ZIF-8 self-assembles into two prominent morphologies: sodalite (SOD), which has a rhombic dodecahedral morphology, and diamondoid (dia), a collection of flat, stacked crystals of diamond cubic morphologies.<sup>12</sup> ZIF-8 SOD is the kinetic product and has a large pore size (3.4 Å) and high thermal stability and surface area (BET: 1630 m<sup>2</sup> g<sup>-1</sup>).<sup>17</sup> ZIF-8 dia is the thermodynamic product as discovered by mechanochemical milling of ZIF-8 SOD. 12 ZIF-8 dia has the same secondary building units (SBUs) as SOD but grows into a nonporous 1D channel that has hexagonal structures that intersect with other channels to create the 3D dia topology. Although the SBUs of these two polymorphs are identical, their topology and porosity differ and influence their functionality and biomolecule encapsulation. 18 ZIF-8 has been thoroughly investigated due to its facile synthesis under aqueous conditions at room temperature. However, the molecular origin of the polymorph control in ZIF-8 is still unknown.

In this report, we investigate the polymorph control of ZIF-8 through variation in the ligand (2-methylimidazole) to metal (zinc acetate) ratio. A combination of scanning electron microscopy (SEM) and powder X-ray diffraction (PXRD) aids in understanding the topology and morphology that are observed in ZIF-8 polymorphs. Time-resolved electrospray ionization mass spectrometry (ESI-MS) and cryogenic transmission electron microscopy (cryo-TEM) are used to understand the prenucleation cluster composition and structure prior to polymorph formation. In situ wide-angle X-ray scattering (WAXS) is used to uncover the rate of crystallization during polymorph formation.

#### RESULTS

**ZIF-8 Synthesis.** Stock solutions of HmIm (160, 700, and 1400 mM 1 mL) and zinc acetate (40, 1 mL) were prepared with Milli-Q water. Stock solutions were used to prepare a series of MOF crystallization experiments with variation in the HmIm/Zn ratio (4:1, 17.5:1, and 35:1). The solutions were combined without mixing and aged for 24 h. The precipitate was obtained by centrifugation at 10,000 rpm for 10 min. The precipitates were washed with Milli-Q water and centrifuged three times prior to Cyro-TEM and powder PXRD analysis.

Polymorph Characterization. To characterize the polymorph formation at HmIm:Zn ratios of 4:1, 17.5:1, and 35:1, bulk analysis was carried out by PXRD of the final crystals collected by centrifugation after 24 h of reaction. ZIF-8 4:1 diffraction peaks appear around  $2\theta$  of 12.4, 12.9, and 13.6° that relate to the dia polymorph. 35:1 displays diffraction peaks around  $2\theta$  of 7, 10.2, and  $12.7^{\circ}$  that relate to the simulated SOD PXRD pattern. 17.5:1 reveals that both of the PXRD patterns for SOD and dia can be observed with a slight preference for dia morphology as the SOD peaks are much less intense. SEM was used to analyze the morphologies of the different polymorphs. SEM of the 4:1 ratio revealed that only the dia polymorph for ZIF-8 is defined by larger crystals, ranging in size around 3  $\mu$ m (Figure 1a). With an increase in ratio to 35:1, the surfaces become more faceted and represent the truncated dodecahedral structure of SOD (Figure 1b). The 17.5:1 ratio displays a mix of both polymorphs in equal distributions, with the dia crystals being significantly larger and varying in size compared to the smaller, more uniform SOD crystals (Figure 1c). Intermediate ranges of HmIm:Zn ratios were compared to identify the amount of SOD and dia present

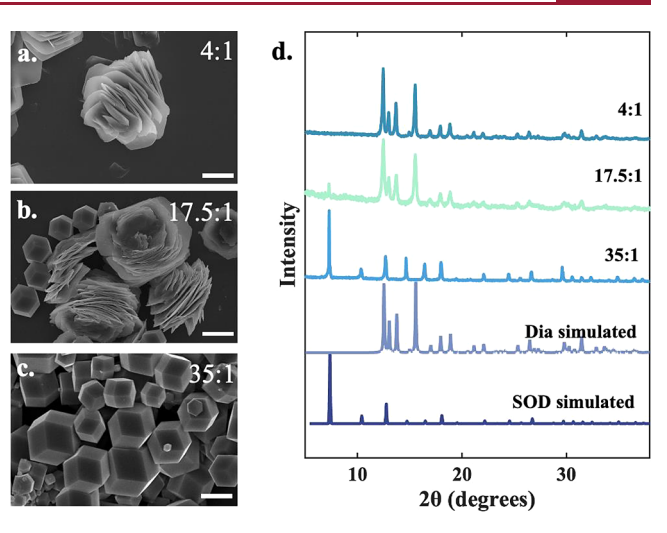


**Figure 1.** SEM of ZIF-8 (a) 4:1, (b) 17.5:1, (c) 35:1 (all scale bars are 2  $\mu$ m), and (d) PXRD of ZIF-8 at HmIm:Zn ratios of 4:1, 17.5:1, and 35:1, and simulated patterns for SOD and dia.

in the final crystals and it was shown that the amount of SOD character increases with HmIm increase (Figure S5).

Crystal size analysis of the final crystals was performed to determine the size and polydispersity of each of these polymorphs (Table 1). 35:1 contains much smaller crystals

Table 1. Summary of Crystal Sizes of ZIF-8 at Three Different HmIm Ratios (35:1, 17.5:1, and 4:1)

HmIm:Zn (mM:mM)	ratio HmIm:Zn	crystal size SOD (nm)	crystal size dia (nm)
80:20	4:1		$5500 \pm 1100$
350:20	17.5:1	$1700 \pm 390$	$3500 \pm 1100$
700:20	35:1	$2200 \pm 810$	

than that of dia and also has a smaller size distribution showing more uniform crystals. 17.5:1 displays smaller dia crystals that are seen in 4:1 and slightly smaller (2000 nm) SOD crystals. This is consistent with previous studies that show as you increase the HmIm ratio the polydispersity decreases.  $^{13}$ 

In Situ X-ray Scattering. In situ WAXS was utilized to understand the time-resolved crystallization kinetics of ZIF-8. To gain information about the rate of crystallinity, experiments were performed using an in-house X-ray source, monitoring  $6.5-7.5^{\circ}$  2 $\theta$  every 10 min for 24 h. Following measurements, the data was normalized against the background, and the integrated intensity was plotted to determine the extent of crystallization (Figure 2a). The ZIF-8 solutions were prepared by mixing HmIm and Zn precursors at 35:1 and 4:1 ratios and were immediately placed in 1 mm special glass capillaries. We define t = 0 as the time of mixing, and the first collected data point is 10 min. 35:1 ZIF-8 reaches full extent of crystallization at around 3 h. 4:1 ZIF-8 takes around 8 h to begin to plateau in crystallinity and does not completely flatten by the end of the collection time around 12 h. In-house X-ray sources were ideal for long collection times, but the time resolution and collection angle were limited by the intensity of the X-ray source. To achieve a higher temporal resolution, synchrotron-based in situ WAXS was utilized to collect the entire spectrum of  $5-40^{\circ} 2\theta$ in 1 s.

In situ WAXS experiments were performed on the 7.3.3 beamline of the Advanced Light Source (ALS) at Lawrence

Crystal Growth & Design pubs.acs.org/crystal Article

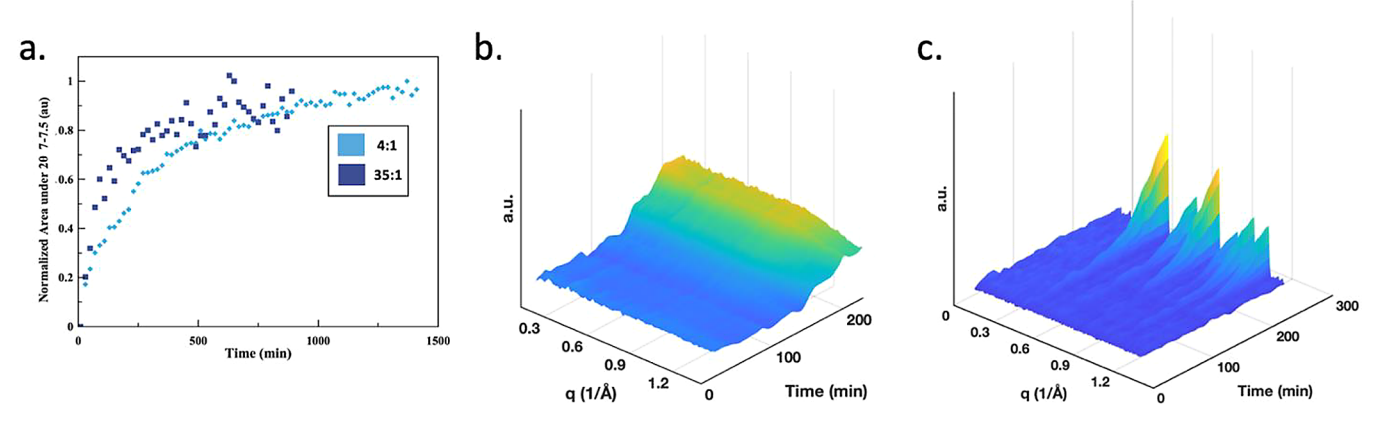


Figure 2. (a) Plot of the normalized area under  $2\theta$  7–7.5 versus time produced by the integrated intensity of the (211) reflections collected by time-resolved in situ XRD. Time-resolved wide-angle X-ray scattering patterns of ZIF-8 (b) 4:1 and (c) 35:1 for the first 250 min. Background subtraction was performed for (c) using an in-house MATLAB script, see Supporting Information for details.

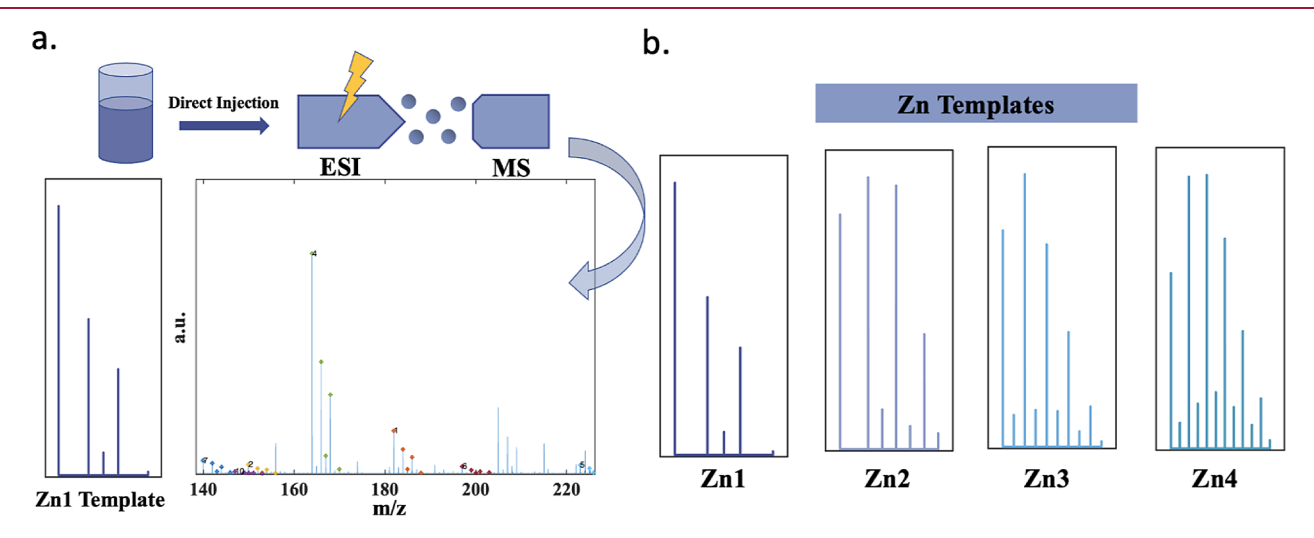


Figure 3. (a) ESI source where a dilute solution of ZIF-8 is injected, electrosprayed, and projected toward the MS inlet, yielding relative abundance versus mass/charge. Automated peak analysis shows the intensity of n Zn oligomers with sizes n = 1-4, (b) Zn fragmentation patterns of n Zn oligomers with sizes n = 1-4.

Berkeley National Laboratory (Berkeley, CA). The ZIF-8 reaction was initiated through mixing precursor solutions in a glass vial, and the solutions were immediately placed in a 1 mm quartz capillary. The capillary was then mounted into the instrument over the course of 5 min. The data collection began once the sample was mounted. We define t = 0 as the time of mixing, and the first data was collected at t = 10 min. Figure 2b,c shows the WAXS plots of HmIm:Zn ratios of 4:1 and 35:1 respectively, over the reaction time of 4 h. The peaks that are present in 35:1 after 150 min are related to the lattice for ZIF-8 SOD. The spectrum for 4:1 does not show any significant peaks but an increase in overall intensity after the 4 h collection period. This is not consistent with the in-house collected WAXS which shows an increase in intensity of the  $6.5-7.5^{\circ}$  2 $\theta$ . This could be due to the lack of range in which the in-house WAXS could collect in comparison to the synchrotron-based WAXS, and therefore could include some of the formation of amorphous phases which can cause an increase in intensity. This wider range data allows us to understand that in the first 4 h, significant nucleation occurs in the 35:1 system but not in the 4:1 system.

**Mass Spectroscopy.** To gain a better understanding of the species present during the initial stage of nucleation under

different precursor conditions, the relative abundance of different Zn clusters was determined from time-resolved ESI-MS. This methodology was adapted from previous work which studied the evolution of Zn clusters for understanding the nucleation and growth of ZIF-67.

The ESI-MS data was analyzed using an in-house MATLAB script developed to automatically identify characteristic PNC fragmentation patterns in the data based on simulated fragmentation patterns of Zn in solution (Figure 3b). nZn fragments were simulated from n = 1-4 which displayed distinct isotope patterns. Zn clusters larger than 4Zn were difficult to distinguish, so the analysis is capped at 4Zn. The maximum peaks from each characteristic fragmentation pattern were integrated and summed to determine the total amount of PNC present in each ESI-MS data set (Figure 3). The crystallization solutions were mixed for 5 time points running from 1 min to 12 h and at the desired reaction time, diluted by 100x to stop reaction as well as prepare the solution for mass spectroscopy appropriate concentrations (Figure 4a-c). Time points after 12 h were not collected due to a decrease in signal observed after 12 h as the clusters moved from prenucleation to bulk crystal phases.<sup>11</sup> As ZIF-8 crystallizes, the precipitates crash out of solution and sink toward the bottom of the

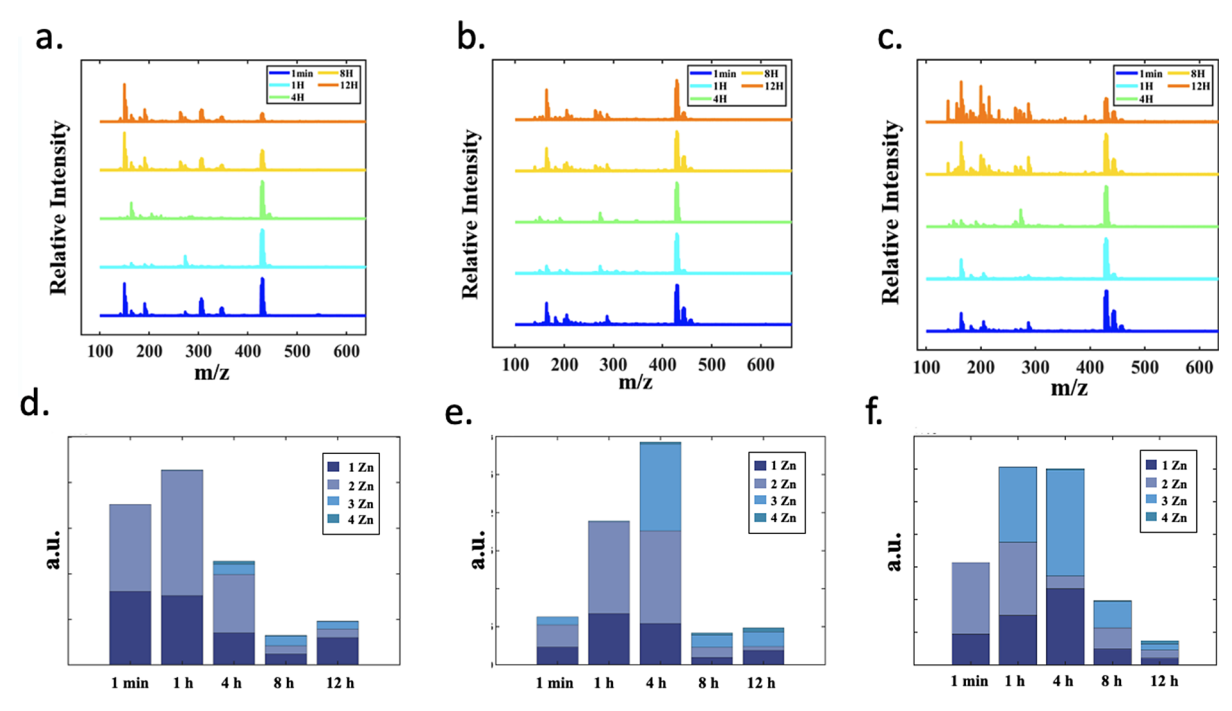


Figure 4. Stacked ESI-MS plots of ZIF-8 at times 1 min, 1 h, 4 h, 8 h, and 12 h at Zn: HmIm ratio of (a) 4:1, (b) 17:5:1, and (c) 35:1. Sum of peaks of Zn oligomer size for Zn:HmIm ratios of (d) 4:1, (e) 17:5:1, and (f) 35:1.

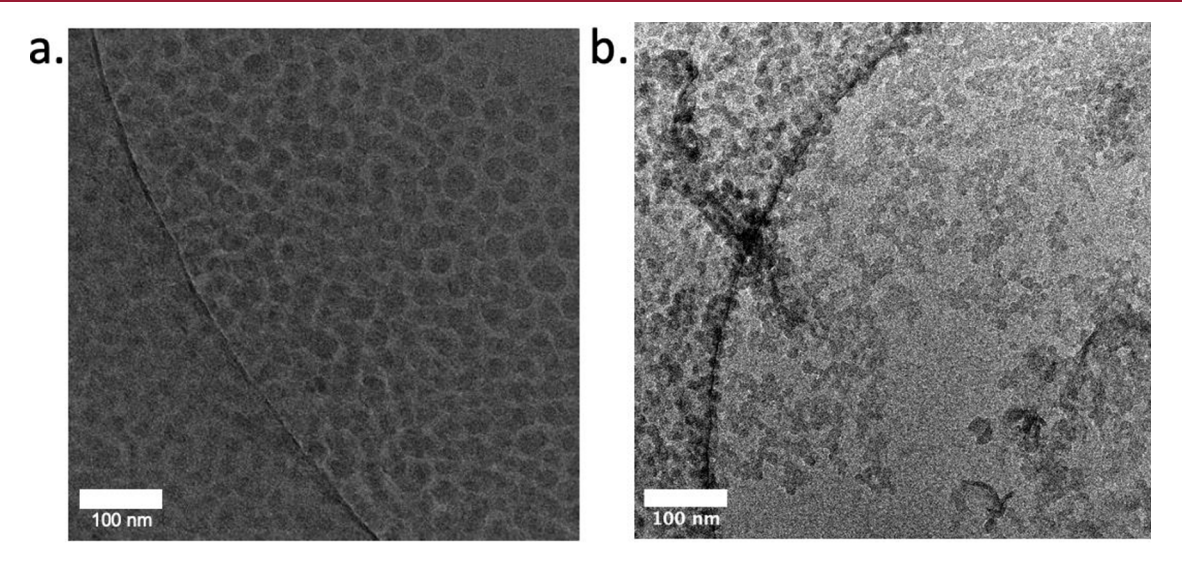


Figure 5. Representative Cryo-TEM images of nucleation and growth at 1 h of ZIF-8 in water. Scale bars are 100 nm. ZIF-8 with precursor ratios of (a) 4:1, (b) 17.5:1.

reaction vial, to ensure that a majority of the sample is the PNCs and not the bulk phases, the samples are taken from the top of the reaction vessel.

After the Zn clusters were assigned, the sum of each Zn cluster intensity was calculated at each sampling interval to show the change in Zn cluster composition as the reaction progressed (Figure 4d-f). The 4:1 ratio showed exclusively 1Zn and 2Zn clusters at 1 h and predominantly 1Zn and 2Zn clusters at 4 h with only 10% of the clusters represented by 3Zn and 4Zn, respectively (Figure 4d). In comparison, 35:1 showed the development of 3Zn as soon as 1 h into the reaction, and the majority of the solution consists of 3Zn at 4 h (Figure 4f). At the 8 h time point, the abundance of Zn clusters decreases to less than the initial abundances indicating that the majority of Zn PNCs are no longer present in the

solution and have crystallized into ZIF-8 SOD. This continues to 12 h where there is half of the abundance of Zn clusters observed in 8 h. The 17.5:1 system indicates an intermediate between the 4:1 and 35:1, with 2Zn not appearing in large abundances until 4 h but still showing a large decrease in Zn clusters around 8 h, indicating that many of the Zn clusters have left the prenucleation phase (Figure 4e). This is supported by the WAXS data that show an increase in crystallinity as the prenucleation cluster concentration decreases (Figure 2). Precautions were taken to ensure that little of the bulk crystal was sampled, but it is possible that the solution sampled contains some larger Zn clusters that have fragmented. Although there may be a mixture of prenucleation species and fragmented species in the sample, there is a clear

trend in the concentration of Zn clusters that demonstrates the presence of PNCs.

**Cryo-TEM.** Cryo-TEM was used to compare the structure of the amorphous precursor particles at 1 h of reaction time. 4:1 (Figure 5a) shows <100 nm spherical particles that appear to be stable to aggregation. 17.5 (Figure 5b) shows smaller particles but they appear to be highly aggregated. Although 17.5:1 at 1 h of reaction shows aggregation, based on the spherical morphology and our previous data on ZIF-8,(ref alana) we interpret these to be amorphous particles. Crystallinity of ZIF-8 at early time points was showcased in a previous publication from our lab. This work shows a crystallinity of 35:1 at the 1 min time point through diffraction patterns and faceted crystals. The cryo-TEM images for 17.5:1 appear to be similar to those of previous studies of aggregation that did not display crystallinity.

# DISCUSSION

The collective data show that the formation of ZIF-8 SOD and dia occurs via the formation of PNCs which aggregate into spherical amorphous particles. SOD crystallization occurs more rapidly than dia, as supported by the in situ X-ray studies. The formation of SOD occurs through the rapid aggregation of particles (cryo-TEM), which results in the formation of 3Zn clusters (ESI-MS). In contrast, the formation of dia occurs via the formation of particles that are more stable to aggregation (cryo-TEM) and results in the formation of 2Zn clusters (ESI-MS). This would indicate that the ratedetermining steps in the nucleation of dia and SOD occur through the reaction of the 2Zn and 3Zn clusters, respectively. This reaction could be through the addition of another Zn or through the aggregation of the 2Zn and 3Zn clusters (Figure S6). The main difference between the dia and SOD synthesis is that for the latter, there is a much greater concentration of ligand. The excess ligand appears to be responsible for the rapid formation of 3Zn clusters and the rapid aggregation of amorphous particles, both of which lead to the nucleation of the SOD polymorph. Specifically, how the excess ligand controls these phenomena remains an open question requiring further investigation.

## CONCLUSIONS

This study of the early stages of nucleation and growth demonstrates the importance of studying the PNCs of ZIF-8 to understand the polymorph control. The main challenge that we address in this study is a molecular understanding of the PNCs and their role in the final polymorph formation. To address this challenge, we utilized complementary methods to study the formation of ZIF-8 through the stages of nucleation and growth, and the combination of these techniques allowed for a more complete picture understanding of polymorph control in ZIF-8 systems. The combined data revealed that SOD nucleates rapidly via the formation and aggregation of amorphous particles that contain a significant amount of 3Zn clusters, whereas dia nucleates more slowly via the formation of stable amorphous particles that are composed of 2Zn clusters.

## METHODS

**Materials.** All chemical reagents used for ZIF-8 were obtained from Sigma-Aldrich and were used without further purification unless stated otherwise. Stock solutions of bovine serum albumin, b-cyclodextrin, 2-methylimidazole (HmIm), and zinc acetate (Zn) were

made using Milli-Q water (18MW). Glass capillaries were obtained from Hampton Research.

Article

**ZIF-8 Synthesis.** Stock solutions of 2-methylimidazole (HmIm) (1400, 700, and 160 mM, 1 mL) and zinc acetate (Zn) (40 mM, 1 mL) were prepared in water ( $\rho$  > 18 M $\Omega$  cm). Stock solutions were then used to prepare a series of crystallization experiments with variation in the HmIm:Zn ratio (35:1, 17.5:1, and 4:1) Zinc acetate solution was added to 2-methylimidazole solutions and crystallization was initiated. The solutions were aged for 24 h at room temperature without stirring and the precipitate was obtained via centrifugation at 10,000 rpm for 10 min. The precipitate was washed by water and centrifuged twice more and a final rinse with methanol.

**SEM.** Samples were prepared by pipetting 10uL of diluted MOF sample onto 1 mm thick glass slides, which were then coated with 5 nm iridium (Quorum Q150T) to reduce charging. Samples were imaged with Magellan 400 XRH system with secondary electron images taken at an accelerating current ranging from 2 to 3 keV.

**Cryo-TEM.** Cryo-TEM samples were prepared using Quantifoil R2/2 Holey Carbon Films from Electron Microscopy Sciences or 400 Mesh Carbon grids from TedPella. Prior to sample application, glow discharge was applied to the grids for 70 s. Reaction solutions at various time points were centrifuged for  $\sim$ 2 s, and 3  $\mu$ L of each sample was taken from the reaction solutions and underwent vitrification using an Automatic Plunge Freezer ME GP2 (Leica Microsystems). Vitrification was performed at  $\sim$  95% humidity with a blot time of 4 s, and samples were plunged into liquid propane. Samples were then analyzed using a JEOL-2100 TEM instrument with a Schottky field-type emission gun set to 200 kV. Images were obtained using Digital Micrograph software or a Gatan OneView Camera.

**PXRD.** After all liquid from the top of centrifuged crystal precipitates was removed and samples were allowed to air-dry, a Rigaku SmartLab X-ray diffractometer was used to obtain the PXRD pattern at 40 kV and 30 mA. Results were plotted with background subtraction using IGOR software.

In Situ WAXS (UCI IMRI). MOF samples were prepared and immediately after mixing were loaded into 1 mm special glass capillaries. All measurements were performed on a Rigaku SmartLab X-ray diffractometer was used to obtain a PXRD pattern at 40 kV and 30 mA scanning from  $2\theta$  6.5–7.5°. Results were plotted and analyzed in Matlab using an in-house script.

In Situ WAXS (LBNL ALS). WAXS samples were prepared in 2 mL quantities as described in the ZIF-8 synthesis, and immediately after mixing the solutions were added to 2 mm in diameter special glass capillaries (10  $\mu$ m wall thickness) and mounted onto a custom built sample holder. The solutions were mounted horizontally to ensure that the entire width of the capillary was being sampled. In situ WAXS data was collected at the SAXSWAXS beamline (7.3.3) at the ALS, Lawrence Berkeley National Laboratory, using a photon energy of 10 keV (wavelength = 1.24 Å). Measurements were taken place at ambient temperatures. Data was collected by a Dectris Pilatus 2 M detector with a pixel size of  $0.172 \times 0.172$  mm, and  $1475 \times 1679$ pixels was used to capture the 2D scattering patterns at a distance of 300 mm from the sample. A silver behenate standard was used as a calibrant. Data was analyzed using the Nika package for Igor Pro. 15 Background subtraction was performed via an in-house MATLAB script (see the Supporting Information for details).

**ESI-MS.** Spectra were recorded on a Xevo G2-XS QTOF (Waters Corporation, Massachusetts, U.S) in positive ion mode. ZIF-8 solutions were mixed to make various HmIm:Zn ratios and were diluted 100x to reach MS appropriate concentrations at time points of 1 min, 1 h, 4 h, 8 h, and 12 h. Samples were electrosprayed using a syringe pump at a flow of 0.1 mL/min coupled to an ion max source set to 3.5 kV spray voltage. A mass range of 100–2000 *m/z* was used.<sup>20</sup> After each sample, a reference of pure water was collected for data correction. An in-house MATLAB script was developed to identify characteristic PNC fragmentation patterns based on simulated fragmentation patterns. Each simulated fragmentation pattern was analyzed individually. The script first identified all possible peak combinations that had the characteristic spacing found

in the simulated data within an error of  $0.01\ m/z$ . For each valid peak combination, the "goodness of match" was determined by calculating the mean square error between the normalized peak heights of the valid peak combination and the normalized peak heights of the simulated fragmentation pattern. The top matches were manually checked, and any anomalous matches were removed from the analysis, allowing preference for higher ranking matches.

### ASSOCIATED CONTENT

## **5** Supporting Information

The Supporting Information is available free of charge at https://pubs.acs.org/doi/10.1021/acs.cgd.4c00194.

Simulated data for Zn isotope patterns; WAXS analysis of 4:1 and 35:1 ZIF-8 after 12 h of reaction; details on background subtraction of WAXS analysis, PXRD patterns ZIF-8 at varying HmIm/Zn ratios; estimated ESI-MS cluster analysis of secondary building units; and methods for particle size analysis (PDF)

#### AUTHOR INFORMATION

#### **Corresponding Author**

Joseph P. Patterson — Department of Chemistry, University of California, Irvine, Irvine, California 92697-2025, United States; Department of Materials Science and Engineering, University of California, Irvine, Irvine, California 92697-2025, United States; ◎ orcid.org/0000-0002-1975-1854; Email: patters3@uci.edu

# **Authors**

- A. Rain Talosig Department of Chemistry, University of California, Irvine, Irvine, California 92697-2025, United States
- Fangni Wang Department of Chemistry, University of California, Irvine, Irvine, California 92697-2025, United States; © orcid.org/0009-0002-0739-3460
- Justin T. Mulvey Department of Materials Science and Engineering, University of California, Irvine, Irvine, California 92697-2025, United States; Occid.org/0000-0002-0296-8598
- Brooke P. Carpenter Department of Chemistry, University of California, Irvine, Irvine, California 92697-2025, United States
- Elisa M. Olivas Department of Chemistry, University of California, Irvine, Irvine, California 92697-2025, United States
- Benjamin B. Katz Department of Chemistry, University of California, Irvine, Irvine, California 92697-2025, United States
- Chenhui Zhu Advanced Light Source, Lawrence Berkeley National Laboratory, Berkeley, California 94720, United States

Complete contact information is available at: https://pubs.acs.org/10.1021/acs.cgd.4c00194

#### Notes

The authors declare no competing financial interest.

# ACKNOWLEDGMENTS

This paper was primarily supported by the National Science Foundation CBET Award #2102033. The authors acknowledge the use of facilities and instrumentation at the UC Irvine Materials Research Institute (IMRI), which was supported in part by the National Science Foundation through the UC

Irvine Materials Research Science and Engineering Center (DMR-2011967). The use of BioPACIFIC SAXS instrument was supported by the BioPACIFIC Materials Innovation Platform of the National Science Foundation under Award No. DMR-1933487. We wish to thank the UCI Mass Spectrometry Facility and Ben Katz for assistance with collection and analyses of protein mass spectrometry data. Data were collected on a Waters Acquity UPLC Xevo G2-XS QTOF system (NIH supplemental funding support received by J.S. Nowick (NIGMS GM097562), Vy Y. Duong (NIH GM105938), and O. Cinquin (NIGMS GM102635). Data were analyzed with Waters MassLynx v.4.1 and MATLAB. This research used beamline 7.3.3 of the Advanced Light Source, which is a DOE Office of Science User Facility under contract no. DE-AC02-05CH11231.

## REFERENCES

- (1) Bertolazzo, A. A.; Dhabal, D.; Molinero, V. Polymorph Selection in Zeolite Synthesis Occurs after Nucleation. *J. Phys. Chem. Lett.* **2022**, 13 (4), 977–981.
- (2) Zhou, H. C.; Long, J. R.; Yaghi, O. Chem. Rev. 2012, 112 (2), 673–674.
- (3) Furukawa, H.; Cordova, K. E.; et al. The Chemistry and Applications of Metal-Organic Frameworks. *Science* **2013**, *341*, No. 1230444.
- (4) Matemb Ma Ntep, T. J.; Wahiduzzaman, M.; Laurenz, E.; Cornu, I.; Mouchaham, G.; Dovgaliuk, I.; Nandi, S.; Knop, K.; Jansen, C.; Nouar, F.; Florian, P.; Füldner, G.; Maurin, G.; Janiak, C.; Serre, C. When Polymorphism in Metal—Organic Frameworks Enables Water Sorption Profile Tunability for Enhancing Heat Allocation and Water Harvesting Performance. *Adv. Mater.* 2023, 36, No. 2211302.
- (5) Karadeniz, B.; Žilić, D.; Huskić, I.; Germann, L. S.; Fidelli, A. M.; Muratović, S.; Lončarić, I.; Etter, M.; Dinnebier, R. E.; Barišić, D.; Cindro, N.; Islamoglu, T.; Farha, O. K.; Friščić, T.; Užarević, K. Controlling the Polymorphism and Topology Transformation in Porphyrinic Zirconium Metal—Organic Frameworks via Mechanochemistry. J. Am. Chem. Soc. 2019, 141 (49), 19214—19220.
- (6) Aulakh, D.; Varghese, J. R.; Wriedt, M. The Importance of Polymorphism in Metal—Organic Framework Studies. *Inorg. Chem.* **2015**, *54* (17), 8679–8684.
- (7) Ke, Q.; Duan, Y.; Ji, Y.; Zhao, D.; Zhang, H.; Duan, C.; Li, L.; Wei, Y. Identical Composition and Distinct Performance: How ZIF-8 Polymorphs' Structures Affect the Adsorption/Separation of Ethane and Ethene. *J. Chem. Eng. Data* **2021**, *66* (9), 3483–3492.
- (8) Widmer, R. N.; Lampronti, G. I.; Chibani, S.; Wilson, C. W.; Anzellini, S.; Farsang, S.; Kleppe, A. K.; Casati, N. P. M.; MacLeod, S. G.; Redfern, S. A. T.; Coudert, F.-X.; Bennett, T. D. Rich Polymorphism of a Metal—Organic Framework in Pressure—Temperature Space. J. Am. Chem. Soc. 2019, 141 (23), 9330—9337.
- (9) Carpenter, B. P.; Talosig, A. R.; Rose, B.; Palma, G. D.; Patterson, J. P. Understanding and Controlling the Nucleation and Growth of Metal—Organic Frameworks. *Chem. Soc. Rev.* **2023**, *52* (20), 6918–6937.
- (10) Van Vleet, M. J.; Weng, T.; Li, X.; Schmidt, J. R. In Situ, Time-Resolved, and Mechanistic Studies of Metal-Organic Framework Nucleation and Growth. *Chem. Rev.* **2018**, *118* (7), 3681–3721.
- (11) Filez, M.; Caratelli, C.; Rivera-Torrente, M.; Muniz-Miranda, F.; Hoek, M.; Altelaar, M.; Heck, A. J. R.; Van Speybroeck, V.; Weckhuysen, B. M. Elucidation of the Pre-Nucleation Phase Directing Metal-Organic Framework Formation. *Cell Rep. Phys. Sci.* **2021**, 2 (12), No. 100680.
- (12) Katsenis, A. D.; Puškarić, A.; Štrukil, V.; Mottillo, C.; Julien, P. A.; Užarević, K.; Pham, M.-H.; Do, T.-O.; Kimber, S. A. J.; Lazić, P.; Magdysyuk, O.; Dinnebier, R. E.; Halasz, I.; Friščić, T. In Situ X-Ray Diffraction Monitoring of a Mechanochemical Reaction Reveals a Unique Topology Metal-Organic Framework. *Nat. Commun.* **2015**, *6*, 6662.

- (13) Ogata, A.; Rakowski, A.; Carpenter, B.; Fishman, D.; et al. Direct Observation of Amorphous Precursor Phases in the Nucleation of Protein—Metal—Organic Frameworks. *J. Am. Chem. Soc.* **2020**, *142* (3), 1433—1442.
- (14) Cravillon, J.; Schröder, C. A.; Nayuk, R.; Gummel, J.; Huber, K.; Wiebcke, M. Fast Nucleation and Growth of ZIF-8 Nanocrystals Monitored by Time-Resolved In Situ Small-Angle and Wide-Angle X-Ray Scattering. *Angew. Chem.* **2011**, *50*, 8067–8071.
- (15) Yoreo, J. J. D.; Gilbert, P. U. P. A.; Sommerdijk, N. A. J. M.; Penn, R. L.; Whitelam, S.; Joester, D.; Zhang, H.; Rimer, J. D.; Navrotsky, A.; Banfield, J. F.; Wallace, A. F.; Michel, F. M.; Meldrum, F. C.; Cölfen, H.; Dove, P. M. Crystallization by Particle Attachment in Synthetic, Biogenic, and Geologic Environments. *Science* 2015, 349 (6247), No. aaa6760, DOI: 10.1126/science.aaa6760.
- (16) Chen, B.; Yang, Z.; Zhu, Y.; Xia, Y. Zeolitic Imidazolate Framework Materials: Recent Progress in Synthesis and Applications. *J. Mater. Chem. A* **2014**, 2 (40), 16811–16831.
- (17) Park, K. S.; Ni, Z.; Côté, A. P.; Choi, J. Y.; Huang, R.; Uribe-Romo, F. J.; Chae, H. K.; O'Keeffe, M.; Yaghi, O. M. Exceptional Chemical and Thermal Stability of Zeolitic Imidazolate Frameworks. *Proc. Natl. Acad. Sci. U. S. A.* **2006**, *103* (27), 10186–10191.
- (18) Carpenter, B. P.; Talosig, A. R.; Mulvey, J. T.; Merham, J.; et al. The Role of Molecular Modification and Protein Folding in the Nucleation and Growth of Protein-Metal-Organic Frameworks. *Chem. Mater.* **2022**, 34 (18), 8336–8344.
- (19) Ilavsky, J. Nika: Software for Two-Dimensional Data Reduction. J. Appl. Crystallogr. 2012, 45 (2), 324–328.
- (20) Rosnes, M. H.; Mathieson, J. S.; Törnroos, K. W.; Johnsen, R. E.; Cronin, L.; Dietzel, P. D. C. Electrospray Mass Spectrometry Investigation into the Formation of CPO-27. *Cryst. Growth Des.* **2019**, 19 (4), 2089–2096.